Circulation: Cardiovascular Imaging

ORIGINAL ARTICLE

Molecular Imaging of VWF (von Willebrand Factor) and Platelet Adhesion in Postischemic Impaired Microvascular Reflow

See Editorial by Sinusas

Koya Ozawa, MD, PhD
William Packwood, BS
Oleg Varlamov, PhD
Yue Qi, MD
Aris Xie, MS
Melinda D. Wu, MD
Zaverio Ruggeri, PhD
Jose A. López, MD
Jonathan R. Lindner, MD

BACKGROUND: Complete mechanistic understanding of impaired microvascular reflow after myocardial infarction will likely lead to new therapies for reducing infarct size. Myocardial contrast echocardiography perfusion imaging and molecular imaging were used to evaluate the contribution of microvascular endothelial-associated VWF (von Willebrand factor) and platelet adhesion to microvascular no-reflow.

METHODS AND RESULTS: Myocardial infarction was produced by transient LAD ligation in WT (wild type) mice, WT mice treated with the VWF proteolytic enzyme ADAMTS13 (a disintegrin and metalloproteinase with thrombospondin type 1 motif, member 13), and ADAMTS13-deficient (ADAMTS13–/–) mice. Myocardial contrast echocardiography perfusion imaging and molecular imaging of VWF and platelet GP (glycoprotein) Ibα were performed 30 minutes after ischemia-reperfusion. Infarct size was measured at 3 days. Mortality during ischemia-reperfusion incrementally increased in WT+ADAMTS13, WT, and ADAMTS13–/– mice (14%, 43%, and 63%, respectively; $P<0.05$). For WT mice, molecular imaging signal for platelets and VWF in the postischemic risk area was 4- to 5-fold higher ($P<0.05$) compared with both the remote nonischemic regions or to sham-treated mice. Signal enhancement in the risk area was completely abolished by ADAMTS13 treatment for both platelets (12.8±3.3 versus −1.0±4.4 IU; $P<0.05$) and VWF (13.9±4.0 versus −1.0±3.0 IU; $P<0.05$). ADAMTS13–/– compared with WT mice had 2- to 3-fold higher risk area signal for platelets (33.1±8.5 IU) and VWF (30.9±1.9 IU). Microvascular reflow in the risk area incrementally decreased for WT+ADAMTS13, WT, and ADAMTS13–/– mice ($P<0.05$), whereas infarct size incrementally increased ($P<0.05$).

CONCLUSIONS: Mechanistic information on microvascular no-reflow is possible by combining perfusion and molecular imaging. In reperfused myocardial infarction, excess endothelial-associated VWF and secondary platelet adhesion in the risk area microcirculation contribute to impaired reflow and are modifiable.

Key Words: blood platelet ■ echocardiography ■ molecular imaging ■ myocardial infarction ■ myocardial ischemia

https://www.ahajournals.org/journal/circimaging

CLINICAL PERSPECTIVE

Rapid restoration of epicardial coronary artery flow has been the primary treatment goal for improving outcomes in acute myocardial infarction. Yet, impaired microvascular reperfusion remains an unsolved clinical problem that contributes to expansion of infarct size after intervention. Microvascular no-reflow is complex and multifactorial. In this study, we have integrated information on molecular imaging and perfusion imaging to demonstrate that after ischemia-reperfusion injury, platelet adhesion to the microvascular endothelial surface occurs as a result of excess endothelial VWF (von Willebrand factor) and that this process contributes to impaired microvascular reflow and infarct size. We also show that it is possible to rescue the normal process that removes excess VWF from the endothelial surface with a recombinant form of the enzyme ADAMTS13 (activity of disintegrin and metalloproteinase with a thrombospondin type-1 motif member 13), which could represent a therapy for improving microvascular reflow and reducing infarct size.

In the era of early reperfusion therapy for acute myocardial infarction (MI), impaired microvascular reflow remains an important challenge and influences infarct size and risk for heart failure and death.[1] Microvascular no-reflow after ischemia-reperfusion (IR) is multifactorial,[1,2] yet therapies specifically used for this phenomenon are those that influence vascular tone.[3] Drugs that inhibit platelet aggregation that are used to maintain epicardial artery patency have been shown in some but not all clinical trials to modestly improve post-MI microvascular reflow,[4] suggesting a possible role of platelets in microvascular obstruction. However, there is sparse evidence of in situ microvascular platelet adhesion and aggregation because of the lack of methods for observing this process in vivo.

Ultrasound molecular imaging with microbubbles targeted to the VWF (von Willebrand factor) and to platelets has been developed for studying atherosclerotic disease and provide information exclusively on events that occur at the blood pool-endothelial interface.[5–8] VWF is a large GP (glycoprotein) that is stored in an ultralarge multimeric form in endothelial Weibel-Palade bodies and, upon secretion, circulates in a folded nonactive conformation.[9] Multimeric VWF that remains endothelial associated or is attached to exposed collagen undergoes shear-mediated unfolding with exposure of the A1-binding domain for platelet GPIbα, which mediates adhesion.[9,10] It has been suggested that excess ultralarge multimeric form and secondary microvascular platelet adhesion after myocardial IR could occur through impairment of ADAMTS13 (a disintegrin and metalloproteinase with a thrombospondin type-1 motif, member 13), which proteolytically cleaves VWF multimers.[11] In mice, ADAMTS13 deficiency has been shown to increase infarct size whereas VWF deficiency protective.[12,13] In this study, we used myocardial contrast echocardiography (MCE) perfusion imaging and myocardial microvascular molecular imaging of VWF and platelet-endothelial adhesion to directly evaluate the role of platelet adhesion in impaired microvascular reflow within the risk area early after IR and its influence on subsequent infarct size.

METHODS

Animal Models

The data, analytic methods, and study materials will be made available to other researchers for purposes of reproducing the results or replicating the procedure. The study was approved by the Animal Care and Use Committee at Oregon Health & Science University. The data, analytic methods, and study materials will have been made available to other researchers for purposes of reproducing the results or replicating the procedure. Studies were performed in WT (wild type) C57BL/6 mice, and mice with genetic deletion of ADAMTS13 (ADAMTS13–/–) on a C57Bl/6 background. For all studies, mice were anesthetized with inhaled isoflurane (1.0%–1.5%) and kept euthermic. For contrast imaging studies, catheters were placed in a jugular vein for contrast administration.

In Vivo Imaging Study Design

Protocol 1

Closed-chest myocardial IR with 30 minutes of transient left anterior descending coronary artery (LAD) occlusion was performed in WT mice (n=40), WT mice treated with recombinant full-length human ADAMTS13, 5 μg IV (R&D Systems, Minneapolis, MN) just before IR (n=14), and ADAMTS13–/– mice (n=16). During LAD occlusion, MCE was performed to assess regional perfusion. Between 30 and 60 minutes after reflow, MCE microvascular molecular imaging was performed with microbubbles targeted to GPIbα on adherent platelets and to the A1-domain of endothelial-associated VWF. Imaging with control nontargeted microbubbles was also performed. On completion of molecular imaging, microsphere-derived risk area and infarct area by 2,3,5-triphenyltetrazolium chloride staining were evaluated. Four sham-treated WT mice were also studied.

Protocol 2

To determine whether endothelial-associated VWF and platelet adhesion detected in protocol 1 were associated with impaired microvascular reflow at the same time interval, a similar protocol of myocardial IR was performed in WT mice (n=9), WT mice treated with ADAMTS13 (WT+ADAMTS13; n=3), and in ADAMTS13–/– mice (n=8). MCE perfusion imaging was performed 30 minutes post-reflow, followed by measurement of risk area and histological infarct area.

Protocol 3

To test whether differences in microvascular molecular phenotype and reflow in protocols 1 and 2 influenced ultimate infarct size, myocardial IR using 45 minutes of LAD occlusion was performed in WT mice (n=24), WT+ADAMTS13 mice (n=16), and ADAMTS13–/– mice (n=12). The longer ischemic time was used because of small infarct size found with 30 minutes of ischemia. Three days after IR, transthoracic echocardiography was performed followed by measurement of microsphere-derived risk area and histological infarct area.

Myocardial IR

A closed-chest model of MI was used to negate the known effects of thoracotomy and cardiac exposure on early postreperfusion MCE molecular imaging and microvascular perfusion.[14] Several days before scheduled MI, mice were anesthetized, intubated, and placed on positive pressure mechanical ventilation. A small left lateral thoracotomy was performed to expose the basal anterior wall. An 8-0 prolene suture was placed under the LAD and was left unsecured. The free ends of the suture were exteriorized through the chest wall and left in a subcutaneous position during closure. On a subsequent day, mice were reanesthetized, the suture was exteriorized through a skin incision, and tension was placed on the suture for 30 minutes. Ischemia was confirmed by ST-segment elevation on ECG and wall motion abnormality in the LAD territory on transthoracic echocardiography. Sham-treated animals received a suture without tightening. For protocol 3, because early imaging on the day of MI was not performed, myocardial IR for 45 minutes was performed with open thoracotomy during the initial surgery.

Targeted Microbubble Preparation

Biotinylated lipid-shelled decafluorobutane microbubbles were prepared by sonication of gas-saturated aqueous lipid dispersion of polyoxyethylene-40-stearate (1 mg/mL), distearoylphosphatidylcholine (2 mg/mL), and distearoylphosphatidylethanolamine-PEG (2000) biotin (0.4 mg/mL; Avanti Polar Lipids). Surface conjugation of biotinylated ligands was performed as described previously.[15] Microbubbles targeted to VWF were prepared using a cell-derived biotinylated peptide representing the N-terminal 300 amino acids of GPIbα. Microbubbles targeted to platelet GPIbα were prepared by surface conjugation of dimeric recombinant murine VWF A1 domain (mature VWF amino acids 445–716).[7] Nontargeted microbubbles for control agent signal during molecular imaging and during perfusion imaging were prepared without the distearoylphosphatidylethanolamine-PEG (2000) biotin. Microbubble concentration was measured by electrozone sensing (Multisizer III; Beckman Coulter, Brea, CA).

MCE Perfusion and Molecular Imaging

MCE was performed with a linear-array probe transducer (15L8-S) interfaced with an ultrasound system (Sequoia; Siemens Medical Systems, Mountainview, CA) with a centerline frequency of 7 MHz. The nonlinear fundamental signal component for microbubbles was detected using multipulse phase and amplitude modulation. Imaging was performed in the midventricular short-axis plane, which in all animals encompassed portions of the ischemic risk area. For perfusion imaging, MCE was performed at a mechanical index of 0.18 during continuous intravenous infusion of microbubbles at 5×10^6 min^{-1}. End-systolic images were acquired for 20 cardiac cycles after a 5-frame destructive pulse sequence at a mechanical index of 1.1. Time-intensity data were fit to the function $y=A(1-e^{-\beta t})$, where y is intensity at time t, A is plateau intensity representing relative microvascular blood volume, β is the microvascular flux rate, and the product of A and β is an index of myocardial blood flow.[16] For molecular imaging, end-systolic frames were acquired 8 minutes after IV injection of 5×10^6 targeted or control microbubbles performed in random order. Signal intensity from retained microbubbles alone was determined as previously described by digital subtraction of the signal from the residual freely circulating microbubbles in the blood pool. Intensity was determined from regions of interest placed over the remote nonischemic territory and the microsphere-derived risk area, which was further subdivided into infarct and noninfarct risk area. In sham-treated animals, data were averaged for regions of interest over the anterior and posterior myocardium.

Echocardiography

High-frequency (30 MHz) transthoracic echocardiography (Vevo2100; Visualsonics, Inc, Toronto, Canada) was performed using a parasternal long-axis and parasternal short-axis plane at the basal, mid-left ventricle (LV), and apical imaging planes. LV area at end-systole and end-diastole and fractional area change were measured. Stroke volume was calculated as the product of the LV outflow tract cross-sectional area and time-velocity integral on pulsed-wave Doppler. Global circumferential strain on speckle tracking echo was calculated using the average of all values from each short-axis plane divided into 6 equal regions.

Risk Area and Infarct Area Measurements

The risk area and infarct area were measured as described previously.[17] At the completion of all protocols, the LAD ligature was retightened, and 200 μL of a 1% w/v solution of fluorescently labeled polystyrene microspheres 3 to 8 μm in diameter (Duke Scientific Corp, Palo Alto, CA) was injected in the LV apex and allowed to circulate for 1 minute. The heart was removed and cut into 7 equal-thickness short-axis sections, which were stained with 2,3,5-triphenyltetrazolium chloride. Digital images of the sections were acquired under UV light, and the summed area devoid of fluorescent microspheres for all sections was defined as the total risk area, expressed as a percent of the total LV area. The infarct area on 2,3,5-triphenyltetrazolium chloride staining was expressed as percent of risk area. The risk area and the subdivided infarct and noninfarct risk area on the slice corresponding to MCE imaging was used to define regions of interest for MCE perfusion and molecular imaging analysis, which were defined blinded to condition. Coregistration between the histological and echocardiographic transaxial planes was based on anatomic landmarks, including papillary muscle anatomy and relative LV and right ventricular dimension. For facilitating anatomic registration, after completing contrast-specific echocardiographic imaging for myocardial

Table 1. Weight and Heart Rate Data in Mice Undergoing Ischemia

Morphometric and Heart Rate Data	WT (n=17)	WT+ ADAMTS13 (n=9)	ADAMTS13–/– (n=5)
Weight, g	24.2±3.2	23.9±2.7	23.8±2.6
Baseline HR, min^{-1}	503±68	526±72	510±85
Ischemic HR, min^{-1}	553±56	595±50	570±74
Postreflow HR, min^{-1}	517±35	548±37	545±46
Molecular Imaging HR, min^{-1}	502±39	550±31	507±62

ADAMTS13 indicates a disintegrin and metalloproteinase with a thrombospondin type-1 motif member 13; HR, heart rate; and WT, wild-type.

perfusion or molecular imaging, a short clip using standard 2-dimensional gray scale imaging at 14 MHz was acquired, which provided better spatial resolution.

Immunohistochemistry

After 45 minutes of myocardial IR, or after sham procedure, myocardial blood volume was removed by retrograde aortic perfusion at physiological pressure of isothermic PBS containing 2.5% albumin. Perfusion-fixed short-axis thick slices that included both the risk area and the nonischemic risk area were cut. Immunohistochemistry was performed using rat anti-mouse monoclonal antibody against platelet CD41 (ab33661; Abcam, Cambridge, MA) and secondary staining with donkey anti-rat Cy3-labeled poloyclonal antibody (Jackson Immuno Research, West Grove, PA). Endothelial staining was performed with Alexa Fluor 488-conjugated isolectin GS-IB4 (Invitrogen, Grand Island, NY). Nuclear counterstaining was performed with Hoechst 33342 (Invitrogen). Fluorescent microscopy was performed on a confocal system (TCS SP5; Leica Microsystems, Buffalo Grove, IL).

Statistical Analysis

Statistical analyses were performed using SPSS Statistics (v24.0; IBM Corp, Armonk, NY). Differences in proportions for mortality during IR were analyzed using a χ^2 test. For analyzing infarct size, molecular imaging, and perfusion data, paired tests where used when comparing risk area to remote area, whereas nonpaired tests were performed for comparisons between animal cohorts based on treatment (sham, ischemia, and ischemia with ADAMTS13) and based on strain (WT versus ADAMTS13–/–). Tests for normal versus nonnormal distribution were made using a Shapiro-Wilk test, which for molecular imaging data was applied to residual values. A Student *t* test (paired or unpaired) was performed for comparisons of normally distributed data. For non-normally distributed data, either a Mann-Whitney *U* test or Wilcoxon signed-rank test was used as appropriate according to experimental conditions (group-wise comparisons versus paired data within a group). Comparisons were made between WT mice and either WT+ADAMTS13 or ADAMTS13–/– mice. Differences were considered significant at $P<0.05$.

RESULTS

IR Mortality and Risk Area

Procedure-related mortality during closed-chest IR was the lowest for WT+ADAMTS13 (14%) mice and incrementally increased for untreated WT (43%) and ADAMTS13–/– mice (63%; χ^2; $P=0.027$). Heart rate before, during, and after MI (Table 1), and the size of the risk area during LAD occlusion for either 30 or 45 minutes were similar between mouse strains and treatment assignments (Figure 1A and 1B).

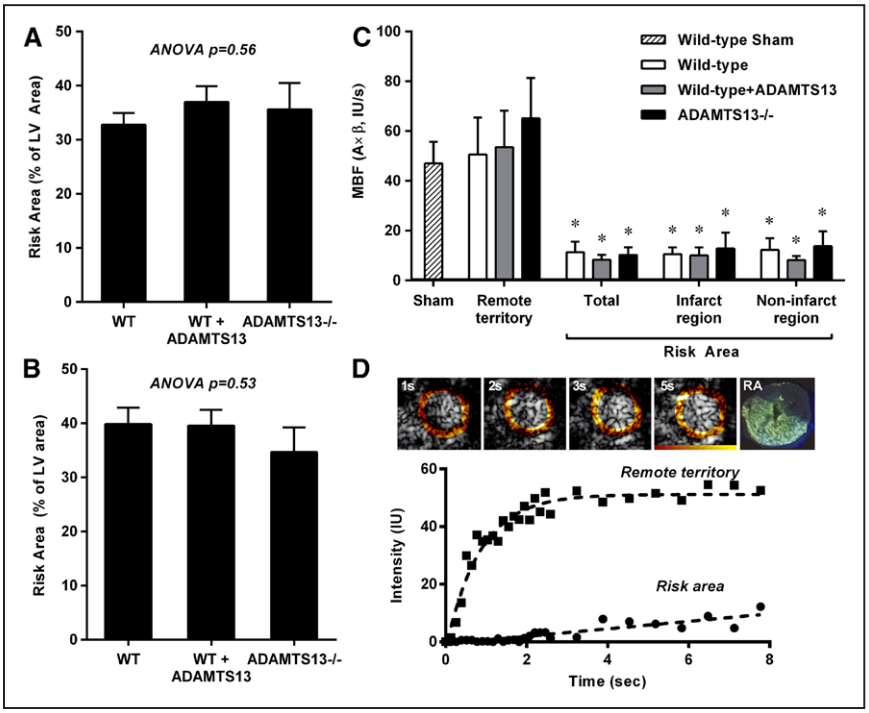

Figure 1. Mean (±SEM) microsphere-derived risk area from animals assigned to either (A) 30 min or (B) 45 min of coronary occlusion.
C, Mean (±SEM) microvascular blood flow from myocardial contrast echocardiography (MCE) performed during coronary occlusion in the risk area and remote territories, as well as from sham-treated mice. **D**, Example of background-subtracted, color-coded MCE images during coronary occlusion, and time-intensity data after a destructive pulse sequence from the risk area and remote territory. For images, time after destructive pulse is at **upper left** and color-coded scale at **bottom** of the 5 s image. ADAMTS13 indicates a disintegrin and metalloproteinase with a thrombospondin type-1 motif member 13; LV, left ventricle; RA, risk area; and WT, wild-type. **P* <0.05 vs remote territory.

Myocardial Perfusion

During LAD occlusion, MCE-derived myocardial microvascular blood flow (MBF) within the microsphere-derived risk area was similar between all groups of mice and was ≈25% of that in the remote territory (Figure 1C). Because mice lack any significant coronary collateral vessels,[18] residual perfusion was likely attributable to critical reduction but not abolishment of antegrade coronary flow. Myocardial MBF during coronary occlusion was similarly reduced when the total risk area was subdivided into the noninfarct risk area and the area destined for infarction. Myocardial MBF in the remote nonischemic territory during coronary occlusion tended to be higher than MBF in sham-treated mice, possibly reflecting greater oxygen demand (ie, from compensatory hyperkinesis or increased wall stress).

In WT mice, myocardial MBF measured 30 minutes after IR was significantly lower in the risk area than the remote territory (Figure 2A). Compared with WT mice, WT+ADAMTS13 mice had a greater degree of microvascular reflow in the risk area whereas ADAMTS13–/– had less reflow. In the WT+ADAMTS13 mice, post-MI MBF was similar for the reperfused risk area and the control nonischemic region. When MBF data were analyzed on a parametric basis, the reduction in perfusion in the risk area in WT was from a decrease in microvascular flux rate (β), whereas ADAMTS13–/– also had a reduction in microvascular blood volume as well (Figure 2B and 2C). The degree of microvascular reflow tended to be greater in the noninfarct risk area than infarcted risk area for all 3 groups of mice (Figure I in the Data Supplement).

Molecular Imaging of VWF and Platelets

On MCE molecular imaging 30 minutes after IR, signal enhancement for active VWF A1 domain and platelet GPIbα was low in both sham-treated mice and in the remote nonischemic territory for all mouse strains and treatment assignments (Figure 3A and 3B). Signal for VWF and platelets was higher in the postischemic risk area than the corresponding remote nonischemic territory for both WT and ADAMTS13–/– mice. In mice treated with recombinant ADAMTS13, there was no significant difference between the risk area and remote territory for either VWF or platelet signal, indicating that ADAMTS13 entirely eliminated selective signal enhancement in the risk area. The risk area signal in ADAMTS13-treated mice was significantly less than in WT and ADAMTS13–/– mice. There were no major differences in molecular imaging signal enhancement for the infarct and noninfarct portions of the risk area (Figure II in the Data Supplement). It is important to note, however, that molecular imaging signal enhancement was not corrected for regional differences in postischemic MBF, which is recognized to influence the number of microbubbles retained and hence signal intensity.[19] Fluorescent immunohistochemistry confirmed the presence of platelet adhesion in the myocardial microcirculation in the postischemic risk area (Figure 4). Platelet adhesion was observed as single events or as linear grouping of platelets, but large aggregates were not observed. Platelet adhesion was absent in control nonischemic mice or in the remote nonischemic regions of mice undergoing IR.

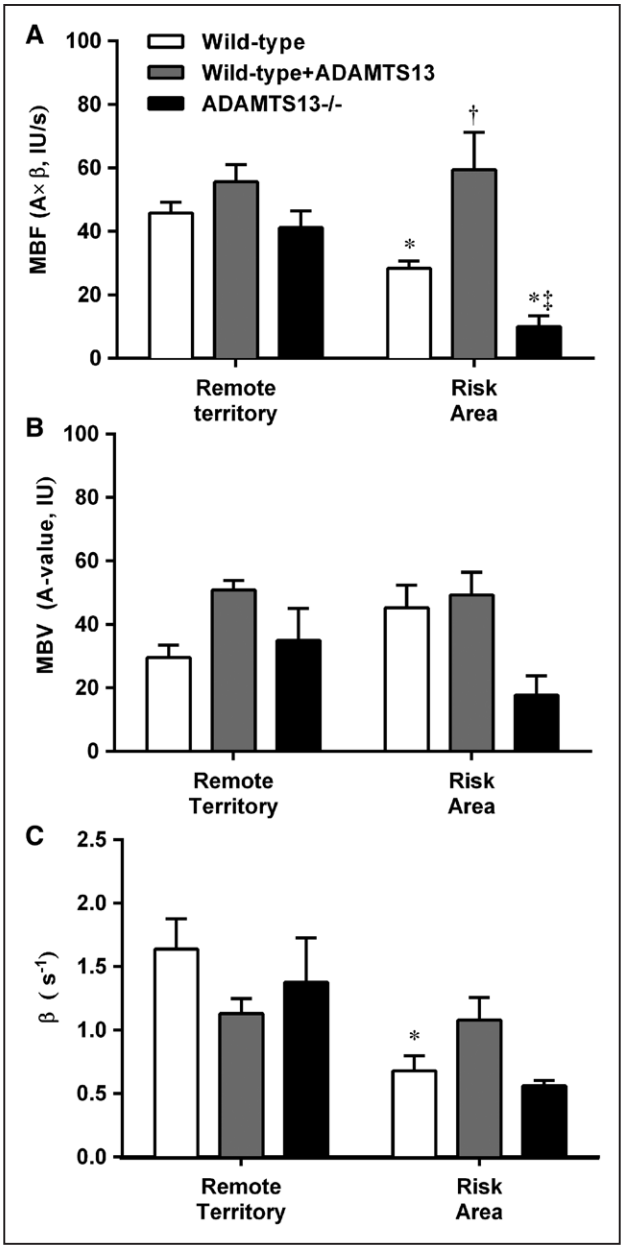

Figure 2. Postischemic myocardial perfusion by MCE in mice undergoing 30 min of ischemia and reperfusion measured in the remote region and the risk area.

Data (mean±SEM) are shown for (**A**) myocardial microvascular blood flow (MBF), (**B**) microvascular blood volume (MBV), and (**C**) microvascular flux rate (β). ADAMTS13 indicates a disintegrin and metalloproteinase with a thrombospondin type-1 motif member 13. **P* <0.05 vs remote territory; †*P* <0.05 vs WT (wild type); ‡*P* <0.05 only before correction for multiple comparison.

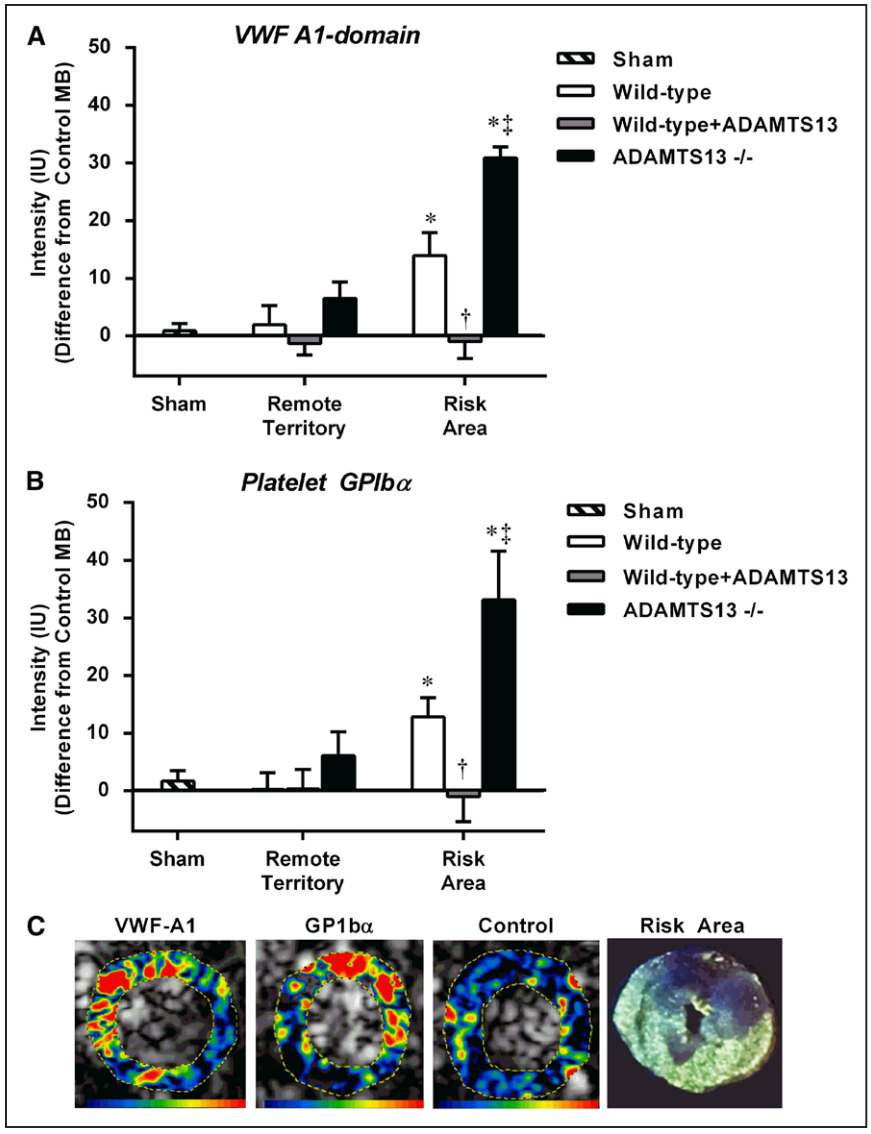

Figure 3. Mean (±SEM) signal enhancement on MCE molecular imaging after 30 min of ischemia and reperfusion for (A) VWF (von Willebrand factor) A-1 domain and (B) platelet GP (glycoprotein) Ibα. Data are expressed as signal difference between targeted and control microbubbles (MB). **C**, Examples of color-coded MCE molecular imaging in the short-axis plane for targeted and control MBs (color scale at **bottom**) and the microsphere-derived risk area in the same short-axis plane. **P* <0.05 vs remote territory; †*P* <0.05 vs wild-type and ADAMTS13–/– (a disintegrin and metalloproteinase with a thrombospondin type-1 motif member 13); ‡*P* <0.05 vs WT (wild type).

Infarct Size and 2-Dimensional Echocardiography

In protocol 3, a longer ischemic duration was used, and infarct size was assessed 3 days after IR to better assess the long-term impact of impaired microvascular reflow. Infarct size as a percentage of the risk area was significantly smaller in WT mice that were treated with ADAMTS13 and was larger in ADAMTS13–/– than WT mice (Figure 5). Despite these differences in infarct size, on echocardiography, fractional area change was similar between groups, and only stroke volume was reduced in ADAMTS13–/– versus WT mice (Table 2).

DISCUSSION

Impaired microvascular reflow after acute MI remains an unresolved issue that contributes to larger infarct size and worse clinical outcomes.[1,20] Imaging techniques that directly assess microvascular integrity have demonstrated poor microvascular reflow in 20% to 35% of patients with reperfused ST-segment–elevation MI, despite having normal thrombolysis in MI flow grades in the epicardial artery.[20,21] Based on the complexity of the many pathways that contribute to the microvascular no-reflow phenomenon, techniques that are capable of directly examining cellular events within the microcirculation would be useful for evaluating the efficacy or futility of targeted therapies. In the current study, we applied molecular imaging techniques capable of evaluating microvascular platelet adhesion in vivo in post-ST-segment–elevation MI no-reflow, which is of interest because it is a potentially modifiable process.

MCE imaging was used in this study to evaluate microvascular platelet adhesion, which can potentially play a multifaceted role in postischemic injury.[22] Platelet adhesion directly to the activated endothelium can occur through many pathways, including fibrinogen or fibronectin cross-bridging of β_3 receptors ($\alpha_v\beta_3$ and $\alpha_{IIB}\beta_3$), by interaction with PSGL-1 (P-selectin glycopro-

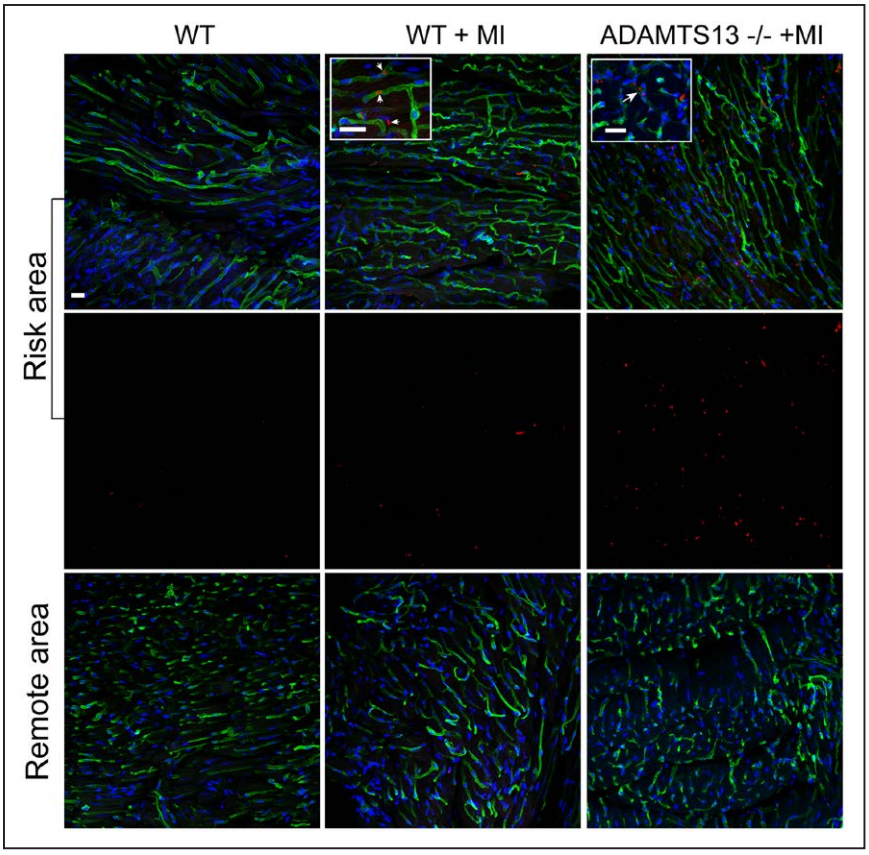

Figure 4. Examples of immunohistochemistry from the sham-treated control WT (wild type) mice (anterior and posterior myocardial with anterior labeled as risk area) and from postischemic WT and ADAMTS13–/– (a disintegrin and metalloproteinase with a thrombospondin type-1 motif member 13) mice.
The **top** and **bottom** rows show fused images for platelet CD41 immunostaining (red), endothelial lectin staining (green), and nuclear counterstain (blue). The middle row shows corresponding images for only the red channel (platelet CD41) in the risk area. For the insets, arrowheads show single platelets, whereas the arrow in the ADAMTS13–/– mouse illustrates 3 platelets linearly arranged (scale bar=20 μm). MI indicates myocardial infarction.

tein ligand-1), and interaction of platelet GPIbα with self-associated ultralarge multimeric form strings or networks that are present on the endothelium. Platelet adhesion and aggregation can lead to increased microvascular resistance directly through luminal obstruction or indirectly either by augmenting the postischemic inflammatory response or by promoting thrombin activity and vasospasm.[22–24] Histology from the current study suggests that in nonthrombotic coronary obstruction and reperfusion, large platelet aggregates do not form but rather platelet adhesion, including in linear arrangements, occur early after reflow within the postischemic risk area.

With regard to the specific role of VWF-mediated platelet recruitment, murine models of myocardial IR have revealed a reduction in infarct size in WT mice treated with recombinant ADAMTS13 and larger infarct size in ADAMS13–/– than WT mice.[12,13] In the latter case, the infarct size in ADAMTS13–/– mice is not increased when there is also deficiency in VWF.[12] These studies have confirmed a role of ADAMTS13 and VWF in determining infarct size in mice. However, these studies did not quantify the degree of microvascular-associated VWF, the degree of platelet adhesion, or their relationship to the patency of the microcirculation. As a result, the mechanism for these strain-dependent differences

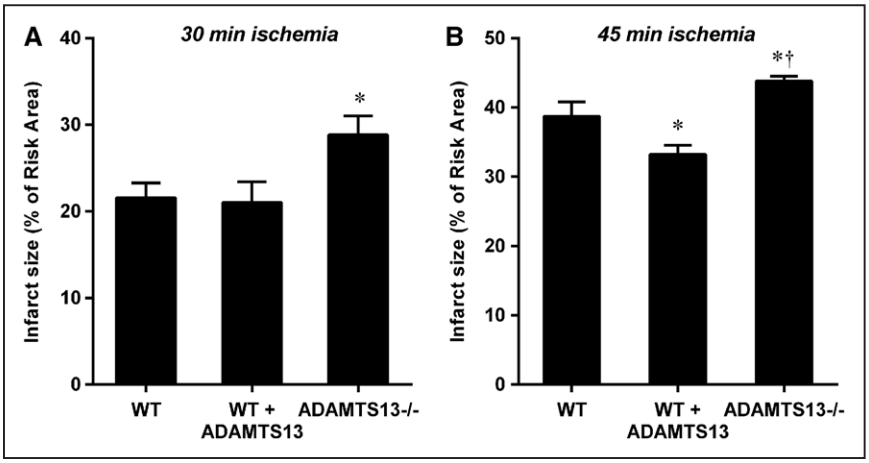

Figure 5. Mean (±SEM) infarct size by triphenyltetrazolium chloride staining as a percentage of the total microsphere-derived risk area for mice undergoing either (A) 30 min of ischemia followed by 90 min of reperfusion or (B) 45 min of ischemia followed by 3 d of reperfusion.
**P* <0.05 vs WT (wild type) before Bonferroni correction; †*P* <0.05 vs WT+ADAMTS13 (a disintegrin and metalloproteinase with a thrombospondin type-1 motif member 13) after Bonferroni correction.

Table 2. Echocardiographic Markers Left Ventricular Function at Day 3 Post-Myocardial Infarction

Echocardiographic Measurements	WT (n=11)	WT+ ADAMTS13 (n=8)	ADAMTS13–/– (n=10)
Stroke volume, μL*	42.7±5.2	37.2±3.5	29.3±2.6†
Fractional area change, %	43.3±1.6	44.8±1.6	42.8±2.0
GCR, %	–17.0±1.3	–16.6±1.6	–17.7±1.9

ADAMTS13 indicates a disintegrin and metalloproteinase with a thrombospondin type-1 motif member 13; GCR, global circumferential strain; and WT, wild type.

*ANOVA, P=0.11.

†P <0.05 for ADAMTS13–/– vs WT on post hoc analysis.

in infarct size has been speculative, although effects on postischemic inflammatory cell recruitment has been suggested.[12,13] Also, the recent finding that intracoronary administration of ADAMTS13 had no effect on infarct size in pigs has created some controversy on the role of VWF in IR injury,[25] although it should be mentioned that this study did not normalize infarct size to risk area; and post-MI ADAMTS13 activity was not impaired unlike what has been described in humans.[26]

Our studies were designed to address uncertainty in the role of VWF regulation and platelet adhesion in microvascular reflow and infarct size and to demonstrate that these processes can be quantified noninvasively with state-of-the-art imaging. We used MCE to assess patency of the microcirculation early after reflow and MCE molecular imaging, which is unique in its ability to examine only events that occur at the interface between the blood pool and the vasculature. Our results provide direct evidence for excess intravascular VWF and platelet adhesion after MI in the entire risk area, which is reduced by exogenous ADAMTS13 and is greater in mice genetically lacking ADAMTS13. On a group-wise basis, greater signal enhancement for VWF and platelets was associated with less microvascular reflow and larger infarct size. The finding that microvascular perfusion in the risk area was restored by recombinant ADAMTS13 strongly suggests that VWF was endothelial-associated rather than collagen-associated because complete normalization of flow after exposure to matrix would be highly unlikely in the latter circumstance. Although the GPIbα receptor for VWF is constitutively expressed and does not require platelet activation, the more activated status of platelets from patients with ST-segment–elevation MI who have no-reflow[27] is likely to be important in terms of converting adhesion to aggregation.

Although the primary purpose of the study was to use molecular imaging to directly link excess endothelial-associated VWF, platelet adhesion, and microvascular no-reflow; our results also suggest that maintaining the ability to proteolytically cleave VWF multimers could represent a targeted therapy for microvascular no-reflow. This idea is underscored by recent first-in-human phase 1 studies of recombinant ADAMTS13 for congenital thrombotic thrombocytopenic purpura.[28] Therapeutic use of ADAMTS13 or other therapies aimed at rescuing VWF proteolytic activity in MI will require much more extensive studies examining the influence of ischemic duration and timing of therapy, as well as models that better recapitulate patients with acute MI.

There are several limitations of this study. We have not elucidated reasons for excess microvascular endothelial-associated VWF. A likely pathway involves heightened oxidative stress during reperfusion injury, which can potentially reduce the activity of ADAMTS13 to cleave VWF at the A2 domain. Although large, group-wise differences were found for platelet and VWF molecular imaging signal, these differences were likely to have been underestimated. This statement is based on the notion that cumulative microbubble entry into tissue is determined by the relative blood flow into the tissue, and groups with the lowest post-MI perfusion also had the highest signal. With regard to clinical translation of our findings, we did not perform studies in the presence of aspirin, heparin, or other antithrombotic agents that are commonly used in patients undergoing primary percutaneous coronary intervention or thrombolytic therapy. Although data are presented for the risk area subdivided into the infarct and noninfarct regions, the limits for spatial resolution of MCE made this analysis difficult. Accordingly, the primary analysis was based on total risk area. It is also important to note that LV function was measured early after MI and may not reflect the long-term consequences of LV remodeling. Finally, mortality rates in the study were higher than expected when performing IR, which we have found to be attributable to the prolonged anesthesia time and volume loads in the form of contrast that was administered in the immediate post-MI period.

In summary, by pairing microvascular perfusion imaging with molecular imaging, we have definitively demonstrated the presence of excess microvascular VWF post-MI, and secondary platelet adhesion. These processes seem to contribute to impaired microvascular reflow and can be potentially modified by strategies that improve ADAMTS13 regulatory activity on endothelial-associated VWF.

ARTICLE INFORMATION

Received April 17, 2018; accepted September 13, 2018.

The Data Supplement is available at https://www.ahajournals.org/doi/suppl/10.1161/CIRCIMAGING.118.007913.

Correspondence

Jonathan R. Lindner, MD, Cardiovascular Division, Oregon Health and Science University, 3181 SW Sam Jackson Park Rd, Portland, OR 97239. Email lindnerj@ohsu.edu

Affiliations

Cardiovascular Division, Knight Cardiovascular Institute (K.O., W.P., Y.Q., A.X., M.D.W., J.R.L.), the Department of Hematology and Oncology, Doernbecher's

Children's Hospital (M.D.W.), and the Division of Cardiometabolic Health, Oregon National Primate Research Center (O.V., J.R.L.), Oregon Health and Science University, Portland. Department of Molecular and Experimental Medicine, Scripps Research Institute, La Jolla, CA (Z.R.). Blood Works NW, Seattle, WA (J.A.L.).

Sources of Funding

Dr Ozawa is supported by a grant from Manpei Suzuki Diabetes Foundation. Dr Lindner is supported by grants R01-HL078610 and R01-HL130046 from the National Institutes of Health (NIH) and a grant (14-14NSBRI1-0025) from the National Aeronautics and Space Administration (NASA) National Space Biomedical Research Institute. Dr López is supported by R01-HL091153 and R01-HL11763 from the NIH. The microscopy core is supported by grant S10-RR024585 from the NIH.

Disclosures

None.

REFERENCES

1. Niccoli G, Scalone G, Lerman A, Crea F. Coronary microvascular obstruction in acute myocardial infarction. *Eur Heart J*. 2016;37:1024–1033. doi: 10.1093/eurheartj/ehv484
2. Reffelmann T, Kloner RA. The no-reflow phenomenon: a basic mechanism of myocardial ischemia and reperfusion. *Basic Res Cardiol*. 2006;101:359–372. doi: 10.1007/s00395-006-0615-2
3. Rezkalla SH, Stankowski RV, Hanna J, Kloner RA. Management of no-reflow phenomenon in the catheterization laboratory. *JACC Cardiovasc Interv*. 2017;10:215–223. doi: 10.1016/j.jcin.2016.11.059
4. Jaffe R, Dick A, Strauss BH. Prevention and treatment of microvascular obstruction-related myocardial injury and coronary no-reflow following percutaneous coronary intervention: a systematic approach. *JACC Cardiovasc Interv*. 2010;3:695–704. doi: 10.1016/j.jcin.2010.05.004
5. McCarty OJ, Conley RB, Shentu W, Tormoen GW, Zha D, Xie A, Qi Y, Zhao Y, Carr C, Belcik T, Keene DR, de Groot PG, Lindner JR. Molecular imaging of activated von Willebrand factor to detect high-risk atherosclerotic phenotype. *JACC Cardiovasc Imaging*. 2010;3:947–955. doi: 10.1016/j.jcmg.2010.06.013
6. Liu Y, Davidson BP, Yue Q, Belcik T, Xie A, Inaba Y, McCarty OJ, Tormoen GW, Zhao Y, Ruggeri ZM, Kaufmann BA, Lindner JR. Molecular imaging of inflammation and platelet adhesion in advanced atherosclerosis effects of antioxidant therapy with NADPH oxidase inhibition. *Circ Cardiovasc Imaging*. 2013;6:74–82. doi: 10.1161/CIRCIMAGING.112.975193
7. Shim CY, Liu YN, Atkinson T, Xie A, Foster T, Davidson BP, Treible M, Qi Y, López JA, Munday A, Ruggeri Z, Lindner JR. Molecular imaging of platelet-endothelial interactions and endothelial von Willebrand factor in early and mid-stage atherosclerosis. *Circ Cardiovasc Imaging*. 2015;8:e002765. doi: 10.1161/CIRCIMAGING.114.002765
8. Schumann PA, Christiansen JP, Quigley RM, McCreery TP, Sweitzer RH, Unger EC, Lindner JR, Matsunaga TO. Targeted-microbubble binding selectively to GPIIb IIIa receptors of platelet thrombi. *Invest Radiol*. 2002;37:587–593. doi: 10.1097/01.RLI.0000031077.17751.B2
9. Ruggeri ZM. Von Willebrand factor, platelets and endothelial cell interactions. *J Thromb Haemost*. 2003;1:1335–1342.
10. Zheng Y, Chen J, López JA. Flow-driven assembly of VWF fibres and webs in in vitro microvessels. *Nat Commun*. 2015;6:7858. doi: 10.1038/ncomms8858
11. Dong JF, Moake JL, Nolasco L, Bernardo A, Arceneaux W, Shrimpton CN, Schade AJ, McIntire LV, Fujikawa K, López JA. ADAMTS-13 rapidly cleaves newly secreted ultralarge von Willebrand factor multimers on the endothelial surface under flowing conditions. *Blood*. 2002;100:4033–4039. doi: 10.1182/blood-2002-05-1401
12. Gandhi C, Motto DG, Jensen M, Lentz SR, Chauhan AK. ADAMTS13 deficiency exacerbates VWF-dependent acute myocardial ischemia/reperfusion injury in mice. *Blood*. 2012;120:5224–5230. doi: 10.1182/blood-2012-06-440255
13. De Meyer SF, Savchenko AS, Haas MS, Schatzberg D, Carroll MC, Schiviz A, Dietrich B, Rottensteiner H, Scheiflinger F, Wagner DD. Protective anti-inflammatory effect of ADAMTS13 on myocardial ischemia/reperfusion injury in mice. *Blood*. 2012;120:5217–5223. doi: 10.1182/blood-2012-06-439935
14. Nossuli TO, Lakshminarayanan V, Baumgarten G, Taffet GE, Ballantyne CM, Michael LH, Entman ML. A chronic mouse model of myocardial ischemia-reperfusion: essential in cytokine studies. *Am J Physiol Heart Circ Physiol*. 2000;278:H1049–H1055. doi: 10.1152/ajpheart.2000.278.4.H1049
15. Lindner JR, Song J, Christiansen J, Klibanov AL, Xu F, Ley K. Ultrasound assessment of inflammation and renal tissue injury with microbubbles targeted to P-selectin. *Circulation*. 2001;104:2107–2112.
16. Wei K, Jayaweera AR, Firoozan S, Linka A, Skyba DM, Kaul S. Quantification of myocardial blood flow with ultrasound-induced destruction of microbubbles administered as a constant venous infusion. *Circulation*. 1998;97:473–483.
17. Mott B, Packwood W, Xie A, Belcik JT, Taylor RP, Zhao Y, Davidson BP, Lindner JR. Echocardiographic ischemic memory imaging through complement-mediated vascular adhesion of phosphatidylserine-containing microbubbles. *JACC Cardiovasc Imaging*. 2016;9:937–946. doi: 10.1016/j.jcmg.2015.11.031
18. Zhang H, Faber JE. De-novo collateral formation following acute myocardial infarction: dependence on CCR2$^+$ bone marrow cells. *J Mol Cell Cardiol*. 2015;87:4–16. doi: 10.1016/j.yjmcc.2015.07.020
19. Carr CL, Qi Y, Davidson B, Chadderdon S, Jayaweera AR, Belcik JT, Benner C, Xie A, Lindner JR. Dysregulated selectin expression and monocyte recruitment during ischemia-related vascular remodeling in diabetes mellitus. *Arterioscler Thromb Vasc Biol*. 2011;31:2526–2533. doi: 10.1161/ATVBAHA.111.230177
20. Ito H, Maruyama A, Iwakura K, Takiuchi S, Masuyama T, Hori M, Higashino Y, Fujii K, Minamino T. Clinical implications of the 'no reflow' phenomenon. A predictor of complications and left ventricular remodeling in reperfused anterior wall myocardial infarction. *Circulation*. 1996;93:223–228.
21. Ito H, Okamura A, Iwakura K, Masuyama T, Hori M, Takiuchi S, Negoro S, Nakatsuchi Y, Taniyama Y, Higashino Y, Fujii K, Minamino T. Myocardial perfusion patterns related to thrombolysis in myocardial infarction perfusion grades after coronary angioplasty in patients with acute anterior wall myocardial infarction. *Circulation*. 1996;93:1993–1999.
22. Gawaz M. Role of platelets in coronary thrombosis and reperfusion of ischemic myocardium. *Cardiovasc Res*. 2004;61:498–511. doi: 10.1016/j.cardiores.2003.11.036
23. Mazzoni MC, Schmid-Schönbein GW. Mechanisms and consequences of cell activation in the microcirculation. *Cardiovasc Res*. 1996;32:709–719.
24. Bombeli T, Schwartz BR, Harlan JM. Adhesion of activated platelets to endothelial cells: evidence for a GPIIbIIIa-dependent bridging mechanism and novel roles for endothelial intercellular adhesion molecule 1 (ICAM-1), alphavbeta3 integrin, and GPIbalpha. *J Exp Med*. 1998;187:329–339.
25. Eerenberg ES, Teunissen PF, van den Born BJ, Meijers JC, Hollander MR, Jansen M, Tijssen R, Beliën JA, van de Ven PM, Aly MF, Kamp O, Niessen HW, Kamphuisen PW, Levi M, van Royen N. The role of ADAMTS13 in acute myocardial infarction: cause or consequence? *Cardiovasc Res*. 2016;111:194–203. doi: 10.1093/cvr/cvw097
26. Kaikita K, Soejima K, Matsukawa M, Nakagaki T, Ogawa H. Reduced von Willebrand factor-cleaving protease (ADAMTS13) activity in acute myocardial infarction. *J Thromb Haemost*. 2006;4:2490–2493. doi: 10.1111/j.1538-7836.2006.02161.x
27. Aurigemma C, Scalone G, Tomai F, Altamura L, De Persio G, Stazi A, Lanza GA, Crea F. Persistent enhanced platelet activation in patients with acute myocardial infarction and coronary microvascular obstruction: clinical implications. *Thromb Haemost*. 2014;111:122–130. doi: 10.1160/TH13-02-0166
28. Scully M, Knöbl P, Kentouche K, Rice L, Windyga J, Schneppenheim R, Kremer Hovinga JA, Kajiwara M, Fujimura Y, Maggiore C, Doralt J, Hibbard C, Martell L, Ewenstein B. Recombinant ADAMTS-13: first-in-human pharmacokinetics and safety in congenital thrombotic thrombocytopenic purpura. *Blood*. 2017;130:2055–2063. doi: 10.1182/blood-2017-06-788026
29. Chen J, Fu X, Wang Y, Ling M, McMullen B, Kulman J, Chung DW, López JA. Oxidative modification of von Willebrand factor by neutrophil oxidants inhibits its cleavage by ADAMTS13. *Blood*. 2010;115:706–712. doi: 10.1182/blood-2009-03-213967
30. Wang Y, Chen J, Ling M, López JA, Chung DW, Fu X. Hypochlorous acid generated by neutrophils inactivates ADAMTS13: an oxidative mechanism for regulating ADAMTS13 proteolytic activity during inflammation. *J Biol Chem*. 2015;290:1422–1431. doi: 10.1074/jbc.M114.599084